Astron. Astrophys. 340, 277–286 (1998)

ASTRONOMY AND ASTROPHYSICS

On the role of beam driven return current instabilities in white-light flares

S.A. Matthews[1], **J.C. Brown**[2], **and L. van Driel-Gesztelyi**[3,4]

[1] Mullard Space Science Laboratory, University College London, Holmbury St. Mary, Surrey RH5 6NT, UK (sam@mssl.ucl.ac.uk)
[2] Department of Physics and Astronomy, University of Glasgow, Glasgow G12 8QQ, UK (john@astro.gla.ac.uk)
[3] DASOP, Observatoire de Paris, F-92195 Meudon Principal Cedex, France
[4] Konkoly Observatory, Pf 67, H-1525 Budapest, Hungary (lvandrie@mesioq.obspm.fr)

Received 9 July 1998 / Accepted 18 September 1998

Abstract. It has been shown previously that the low ionization levels in the deep chromosphere of solar flares can cause the return current driven by a thick target electron beam to be unstable to ion aoustic wave generation, contrary to conventional wisdom. We investigate, using *Yohkoh* data, the possibility that anomalous heating as a result of this instability is capable of producing sufficient heating, in the right places at the right times, to account for the enhanced continuum emission actually observed in white-light flares. The Soft X-ray Telescope (SXT) onboard *Yohkoh* incorporates an aspect camera which, prior to its failure in 1992, provided white-light images at 431 nm with a bandpass of 3 nm. A number of white-light flares were observed during its operational lifetime for which there was coincident hard X-ray data from the Hard X-ray Telescope (HXT), providing suitable candidates for study. Four such events are discussed, and the model found to be viable.

Key words: Sun: activity – Sun: flares – Sun: X-rays, gamma rays

1. Introduction

The problem of accounting for the continuum emission that is observed in solar flares is one which is still largely unresolved. These once seemingly rare events, called white-light flares, place severe constraints on the energy requirements and transport mechanisms operating in the flare (e.g. Neidig 1989), raising the question of whether either partial or total in-situ energy release is required to explain this deep atmospheric heating. Previous ground-based observations of white-light flares (WLFs) have been hampered by various difficulties, including the effects of seeing. The primary disadvantage of this has been the difficulty in obtaining coincident observations in both white-light and X-ray emissions. From this point of view the *Yohkoh* mission provides us with a unique opportunity to observe these events in soft and hard X-rays as well as white-light.

White-light flares are characterized by an increase in emission in the visible range and in integrated light. These enhancements can be seen as patches, waves or ribbons, often with $< 3''$ kernels (Neidig & Cliver 1983, Canfield 1986). In 1989, small aperture patrol telescopes, observing in the range $\lambda < 4000$Å, were reporting about 15 of these events a year near solar maximum. They can be divided into two types according to their spectral features (Machado 1986). Type I events are usually the brightest events and show a Balmer jump at 3600 Å and probably a Paschen discontinuity. The Balmer lines in this type of event are strong and very broad, generally with strong central reversals. Type II events show continuum enhancement with no Balmer jump and weak Balmer lines, with no lines above H11 appearing.

Emission in WLFs has been attributed to either hydrogen free-bound transitions to the second and third levels, i.e. Balmer and Paschen continua, or to H^- emission processes (e.g. Švestka 1986). The first of these emission processes is linked with Type I events, the latter with Type II emission. The emission process relates directly to the location of the WLF source in the atmosphere, and, as a result, constrains the possible heating mechanisms. For Type I events where the emission is considered to be due to bound-free transitions in H, strong heating must occur up to temperatures $\sim 10^4$ K in deep chromospheric layers characterized by $m > 10^{-2}$gcm^{-2} and number densities $n_H > 10^{14}$ cm^{-3} (Machado 1989). These conditions have to be satisfied in order for there to be sufficient opacity in the Paschen continuum region to produce the required brightness enhancement over the photospheric background. This hypothesis has received support from observations of Balmer and Paschen jumps in strong events (Neidig & Wiborg 1984, Neidig 1986). If the emission is due to H^- then the source of the WLF must be in the upper photosphere, below the temperature minimum at $m > 0.1$ g cm^{-2} and $n_H > 10^{16}$ cm^{-3}. Again these conditions are necessary to provide sufficient opacity to produce the observed brightness enhancements with relatively small (~ 100 K) temperature enhancements.

It is widely believed that the energy release in solar flares occurs in the corona and the energy is then transported to the low chromosphere where the optical emission is produced. As a result of this view, attempts to explain the origin of the white-light flare have mostly centred on canonical mechanisms. Neidig

Send offprint requests to: S.A. Matthews

(1989) considered heat conduction as a means of transporting the required energy. He found that assuming that the conductivity is the classical value given by Spitzer (1962), and employing the constant density and pressure assumptions of Schmeleva & Syrovatskii (1973) the temperature gradient required to sustain the required fluxes results in an emission measure at $T < 10^5$ K that is too small to radiate the observed flux, as argued by Brown (1974). According to the thick target model of hard X-ray production (e.g. Brown 1971), the total power in a beam of nonthermal electrons with energy $E \geq 50$ keV is sufficient to power the chromospheric WLF emission (Kane et al. 1986; Canfield et al. 1986). Electrons in this energy range are stopped at a depth in the atmosphere corresponding to $n_H > 10^{13.5} cm^{-3}$, appropriate for chromospheric WLFs. The observed simultaneity between the HXR and WLF emission time profiles (e.g. Neidig & Kane 1993) also lends considerable support to this hypothesis. However, it is highly improbable that electron beams would be capable of producing photospheric WLF emission since this would require electron energies in excess of 900 keV.

There is certainly sufficient total energy associated with a beam of > 4 MeV protons to supply the WLF, but analysis of γ-ray and WLF observations from the July 1 1980 flare by Ryan et al. (1983) has shown that for this flare, thick target heating by energetic protons was insufficient at the time of peak WLF emission. Ryan et al. (1983) and Canfield et al. (1986) also concluded that during the impulsive phase, which occurred well before the WLF emission, the flare could equally well have been powered by protons or electrons. Generally, there is no observed correlation between the γ-ray and WLF emission. Recently, Rieger et al. (1996) have investigated three white-light events using optical data from the Multi-Band Patrol at Sacramento Peak and X-ray and γ-ray observations from the Gamma Ray Spectrometer (GRS) on the Solar Maximum Mission (SMM). They found that for the spectral form of the proton distribution suggested by the measurements, there was insufficient power to account for the WLF emission by at least an order of magnitude. They suggest that if the distribution fits a power law at low energies (c.f. Ramaty et al. 1995, Emslie et al. 1997) or there exists a particle component below 1 MeV which contributes a substantial amount of power then, protons can balance the WLF output. However, their observations do lend support to the concept that the WLF is powered by nonthermal thick target electrons. Simnett (1986) proposed that the bulk of the flare energy went into low energy protons. These are stopped at a relatively low chromospheric density, resulting in explosive heating and a downward propagating compression wave which might produce the WLF. The hard X-rays in this model are suposed to be produced thermally. This possibility can not at present actually be ruled out as it is difficult to distinguish between thermally and non-thermally produced HXR emission and there are few actual diagnostics for low energy protons. However, observations of Hα impact polarization (Hénoux & Chambe 1990, Vogt, Sahal-Brechot & Hénoux 1997, Zhao, Fang & Hénoux 1998) may provide a key to establishing whether low energy protons do play a role.

Alternative possibilities include soft X-ray irradiation ($1-8$ Å). However, at the peak of the WLF emission the power in the 1 - 8 Å range directed towards the solar surface is 10^{-1} of the observed power of the WLF. This makes this a very unlikely mechanism. WLFs are associated with a large EUV flux (McIntosh & Donnelly 1972) of around $6 - 23 \times 10^{27}$ erg s^{-1}; and there is a correlation between the EUV and HXR fluxes. The problem is whether or not EUV photons have a sufficient range in an atmosphere that is normally opaque to EUV radiation. Poland et al. (1988) showed that EUV radiation < 912 Å cannot be the sole energy source but can contribute. Emslie & Sturrock (1997) proposed Alfvén wave dissipation in regions of high resistivity as a means of explaining the heating of the temperature minimum region in ordinary flares (Machado et al. 1978). However, they made no attempt to account for the 10^3 erg cm$^{-3}s^{-1}$ rates which apply in WLFs (Neidig 1989). Delays of several seconds would be expected between the HXR and WLF emission in this case because of the finite wave velocity. Mean delays of approximately 8s have been observed by Neidig & Kane (1993) between the peak of the hard X-rays and the peak of the WLF, although they point out that this lag is within the time resolution of the photographic measurements of six of their events.

The relationship between the hard X-ray flare and white-light emission is one which has received much interest in previous years e.g. Neidig & Kane (1993, Canfield et al.(1986), and is particularly pertinent from the point of view of determining whether the WLF emission is due to energy transport or in situ heating mechanisms. An important limiting factor in beam propagation is that intense enough beams drive a return current faster than the critical speed for electrostatic wave generation. These waves can enhance the resistivity and hence Ohmic energy losses of the beam return current to plasma heating and can act to limit the maximum possible beam flux to the wave generation threshold value (e.g. Brown and Melrose 1977). It has been shown by Matthews, Brown & Melrose (1996) that in the deep layers of the solar chromosphere where the ionization levels are low, the return current can indeed become unstable to the generation of ion-acoustic waves. The associated anomalous resistivity will cause the beam to be decelerated over a very short distance and significant energy deposition to occur at this level of the atmosphere. We investigate the possibility that this energy deposition can account for the observed WLF emission.

2. Collisional beam propagation

If we assume that the beam is collision dominated and adopt a power law spectrum on injection of flux spectral index δ and total flux F_1(cm^{-2}s^{-1}) above cut-off energy E_1, with zero pitch angle, then, allowing for Coulomb scattering and energy losses, Brown's (1972) treatment gives

$$j_b(N) = \begin{cases} F_1 e & N < N_1 \\ F_1 e \left(\frac{N}{N_1}\right)^{(1-\delta)/2} & N \geq N_1 \end{cases} \quad (1)$$

for the beam current at column density N (cm^{-2}) from the injection site. $N_1 = E_1^2/3K$ and the constant $K = 2\pi e^4 \Lambda$ in the Coulomb cross-section K/E^2 has been assumed independent of N. In practice the Coulomb logarithm Λ will decline from its ionized hydrogen value Λ_{ee} of around 20 near the hot injection site to its neutral hydrogen value $\Lambda_{eH} \simeq \Lambda_{ee}/2.6$ in the deep atmosphere.

Beam current neutralization then requires a plasma electron drift current density $j_p = n_e e v_D = -j_b$ at speed v_D where n_e is the electron density given by $n_e = n(x + x_M)$ with n the total (neutral and ionized) hydrogen density, x the degree of hydrogen ionization and x_M a correction for metallic electrons which we take as 10^{-4}. In order for the return current to become unstable to the generation of ion-acoustic waves the drift speed, v_D, must exceed the ion-sound speed, $v_{is} = (kT_e/m_i)^{1/2}$. The calculation of the drift speed necessarily involves a knowledge of the parameters of the electron spectrum, as well as of the atmospheric structure.

With the HXT instrument on *Yohkoh* it is possible to derive spatially resolved spectra for the hard X-ray footpoints corresponding to the kernels of white-light flare emission. In doing this the assumption is made that the photon spectrum is well described by a single power law, and then the spectral parameters A and γ can be calculated for each image in the hard X-ray movie.

The photon spectrum is assumed to have the form:

$$I(\epsilon) = A\epsilon^{-\gamma}\ photons\ cm^{-2}\ s^{-1}\ keV^{-1} \tag{2}$$

If we then also assume that the parent electron spectrum is a power law, viz.,

$$F(E) = F_0 E^{-\delta}\ electrons\ s^{-1}\ keV^{-1} \tag{3}$$

then for thick target emission we can calculate the parameters of the electron spectrum, (F_0, δ) from the photon spectrum viz., (e.g. Hoyng et al. 1976)

$$\begin{aligned} \delta &= \gamma + 1 \\ F_0 &= 4.15 \times 10^{33} A(\gamma - 1)^2 B(\gamma - 1/2, \gamma) E_1^{-\gamma}\ s^{-1} \end{aligned} \tag{4}$$

where $B(\gamma - 1/2, \gamma)$ is the Beta function, E_1 is the cut-off energy of the spectrum and 4.15×10^{33} is a constant.

Following the treatment in Matthews, Brown & Melrose (1996), we have

$$v_D = \frac{F_1 \left(\frac{3KN}{E_1^2}\right)^{1/2(1-\delta)}}{(x + x_M) n_H} \tag{5}$$

where $F_1 = F_0/area$, $K = 2\pi e^4 \Lambda$, N is the column density, E_1 is a cut-off energy, in this case, 25 keV, and δ can be derived from the measured photon spectrum. The area of the electron beam, assuming that the whole of this contributes to the area of the corresponding hard X-ray emission can be calculated from the hard X-ray movie assuming that $S^{3/2} = N_{pix}^{3/2} V_P$. Here S is the area, N_{pix} the number of pixels in the region of interest, and $V_p = 5.7 \times 10^{24}$ cm^3 is the pixel volume (McTiernan et al. 1994).

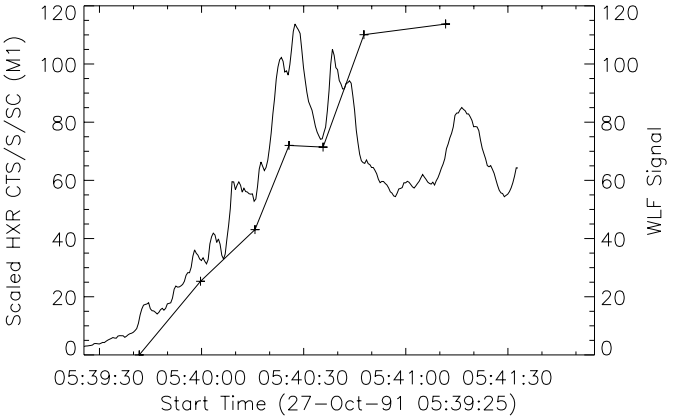

Fig. 1. The temporal variation of the white-light emission (+) and the hard X-ray emission observed in the M2 channel (solid thick line) for the WLF of 27 October 1991.

However, in order to calculate v_D and v_{is} we still require certain parameters of the atmospheric distribution, i.e., the column density, total hydrogen density, degree of ionization and temperature. We take these to be those parameters from the semi-empirical model atmospheres of Basri et al. (1979), model P in the range where we have calculated theoretically that $v_D > v_{is}$. For this level we find that $N = 5.0 \times 10^{20}$cm^{-2}, $n_H = 3.48 \times 10^{13}$cm^{-3}, $x = 1.78 \times 10^{-3}$ and $T = 5.35 \times 10^3$ K. The ratio $R = v_D/v_{is}$ can then be calculated for each time interval of the hard X-ray data and its evolution compared with that of the white-light emission.

3. Observations and data analysis

The aspect camera of the Soft X-ray Telescope (SXT) on board *Yohkoh* (no longer operational) provided white-light images at 431 nm (the CN band) with a bandpass of 3 nm. The image interval is typically 10-12 seconds and this is the first white-light data which has been obtained from outside the Earth's atmosphere, thus providing a unique opportunity to observe WLFs simultaneously in white-light, soft and hard X-rays. Four events observed by *Yohkoh* which exhibited white-light emission have been studied. These events (27 October 1991; 15 November 1991; 26 January 1992 and 14 February 1992) formed part of a white-light survey by Hudson et al. (1994) and van Driel-Gesztelyi et al. (1994). They have also been the subject of studies by other members of the *Yohkoh* team in different wavelength ranges (e.g. Culhane et al. 1993, Kawabata et al. 1994, Yoshimori et al. 1994, McTiernan 1994).

27 October 1991 flare

This event occurred at S13E15 in NOAA active region 6891. The GOES (Geostationary Operational Environmental Satellites) satellite records the start of the flare as 05:37 UT with emission continuing until 07:12 UT. The start of the hard X-ray emission recorded by HXT was 05:47. However, the flare

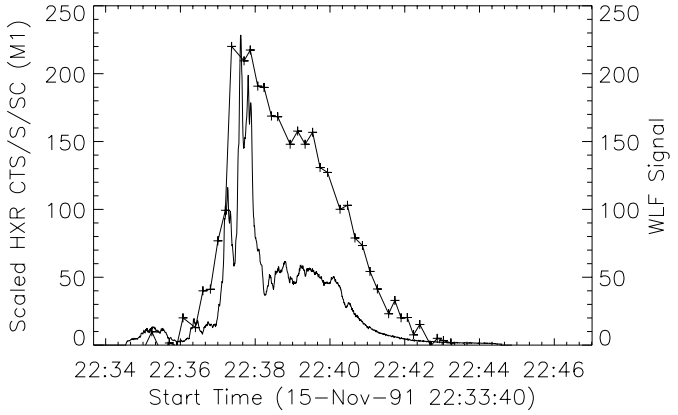

Fig. 2. The temporal variation of the white-light emission (+) and the hard X-ray emission observed in the M2 channel (solid thick line) for the WLF of 15 November 1991.

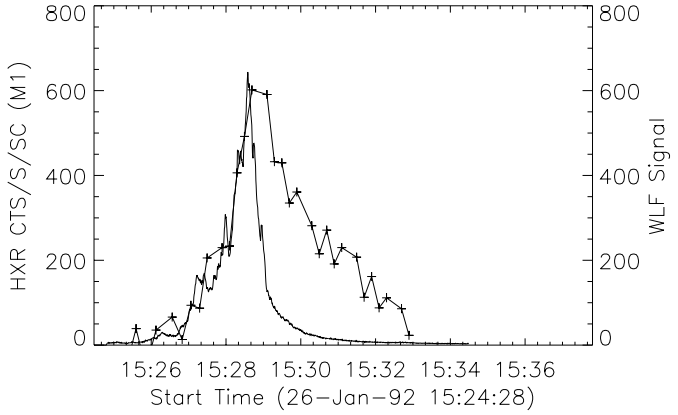

Fig. 3. The temporal variation of the white-light emission (+) and the hard X-ray emission observed in the M2 channel (solid thick line) for the WLF of 26 January 1992.

began in a data gap preceding this time. The GOES class was X6.1 and the Hα importance 3B. This event was also observed by the Nobeyama radioheliograph. The hard X-ray light curve in the M2 channel of the HXT and the white-light light curve for the whole event are shown in Fig. 1. The light curve of the WLF emission is obtained from the difference movie of the WLF. Since the flare both began and ended in a data gap it is difficult to properly define a start time both for the white-light emission and the hard X-ray emission. This may explain the imperfect coincidence between these profiles, particularly at the beginning.

15 November 1991 flare

The event of 15 November 1991 occurred in NOAA active region 6919 at S14W19, commencing at 22:34 UT. The GOES class of this event was X1.5 and the H_α importance 2B. Flare mode was triggered at 24:34:38 UT. As well as white-light emission both γ-ray line and continuum emission were observed from this event. This event was also observed by the Solar X-ray/ Cosmic Gamma-Ray Burst Experiment (Hurley et al. 1992) aboard Ulysses, the hard X-ray and γ-ray spectrometers on PVO, the Compton Gamma ray Observatory and the Nobeyama Radioheliograph. It has been extensively studied in the hard X-ray range by Sakao (1994) and in soft X-rays before saturation of the Bragg Crystal Spectrometer (BCS) at 22:37 UT by Culhane et al. (1993). Again the hard X-ray light curve and light curve for the total white-light emission is shown in Fig. 2. For this event the temporal coincidence between the white-light and hard X-ray emission can be seen to be in excellent agreement.

26 January 1992 flare

This flare occurred in NOAA active region 7012 at S16W66. It commenced at 15:21 UT and had GOES class X1.0 and Hα importance 3B. Flare mode was triggered at 15:24:53 UT. This event was a 'spotless' flare. The relationship between the M2 channel light curve and the WLF light curve is shown in Fig. 3. Again we see that there is very good agreement between the temporal evolution of both the hard X-ray and white-light flares.

14 February 1992

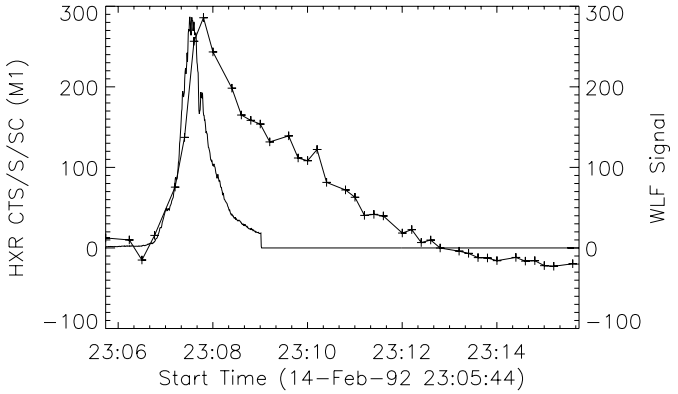

Fig. 4. The temporal variation of the white-light emission (+) and the hard X-ray emission observed in the M2 channel (solid thick line) for the WLF of 14 February 1992.

This flare commenced at 23:04 UT in NOAA active region 7056 at S13E02. It was a GOES class M7.0 event with Hα importance 2B. It was also observed by the Nobeyama Radioheliograph. Fig. 4 shows the HXR light curve in the M2 channel overlaid with the WLF light curve. For this event the start of both emissions is coincident but we later see the hard X-ray emission peak slightly before we observe the peak in white-light.

The preparation of the white-light data is based on the time-wise application of photographic cancellation (Uchida and Hudson 1972). By subtracting a pre-flare image of the active region the white-light emission is easier to detect. Once a series of white-light images has been obtained a light curve can be prepared for each kernel of emission throughout the event. It is important when making light curves to ensure that the area selected around each kernel is the same size to ensure that comparisons between the intensities are meaningful. There is a significant amount of fluctuation in the light curves of the non-flaring regions surrounding the white-light patches and there is no reason to suspect that this is not the case for the areas of enhanced emission as well. For this reason the value of the average background fluctuation in each event is calculated and can be thought of as the error on the light curves for the white-light emission. We

have calculated the start time of the WLF emission to be that time when the light curve exceeds a level of 3σ above a mean background level.

Since we wish to consider the possibility that anomalous heating caused by an unstable return current accompanying a thick target electron beam is responsible for the WLF emission, we have to establish that there is both spatial and temporal coincidence between the WLF emission and the hard X-ray emission. Figs. 1-4 show the hard X-ray light curves overlaid with the light curves of the white-light emission for the whole event. We see that there is indeed a good temporal correlation between the two emissions for the 3 events with good data coverage.

The Hard X-ray Telescope (HXT) on *Yohkoh* is a Fourier synthesis type imager with 64 elements, each measuring a spatially modulated photon count. It is a full Sun instrument providing simultaneous imaging in four energy bands, the L-band (14-23 keV), M1-band (23-33 keV), M2-band (33-53 keV) and H-band (53-93 keV) with an angular resolution of ≈ 5 arcsec and basic temporal resolution of 0.5 seconds (Kosugi et al. 1991). A set of the 64 photon counts is converted into an image with the aid of image synthesis procedures. In this case the image synthesis was performed using an IDL version (Morrison 1994) of a fortran code written by Sakao (1994) which employs a Maximum Entropy algorithm (e.g. Gull and Daniell 1978, Willingdale 1981) to reconstruct the images.

The first step in performing the image reconstruction, after background subtraction, is to accurately determine the flare position on the solar disk in HXT co-ordinates. This enables the synthesis aperture to be defined and the reconstruction proceeds on the premise that no hard X-ray sources contribute to the count rate from outside this field of view. An accurate determination of the flare location is also useful for alignment with soft X-ray images from SXT and hence the white-light images.

Once the image synthesis has been performed on the hard X-ray data the hard X-ray sources can then be identified with the white-light flare kernels. The temporal resolution of the white-light observations is somewhat lower than that of the hard X-ray observations; typically the white-light images are 10-12 seconds apart whilst we have used variable accumulation times to make the hard X-ray images based on a threshold count rate of 2000 counts in the L channel, giving a range of accumulation times from about 1-13 seconds.

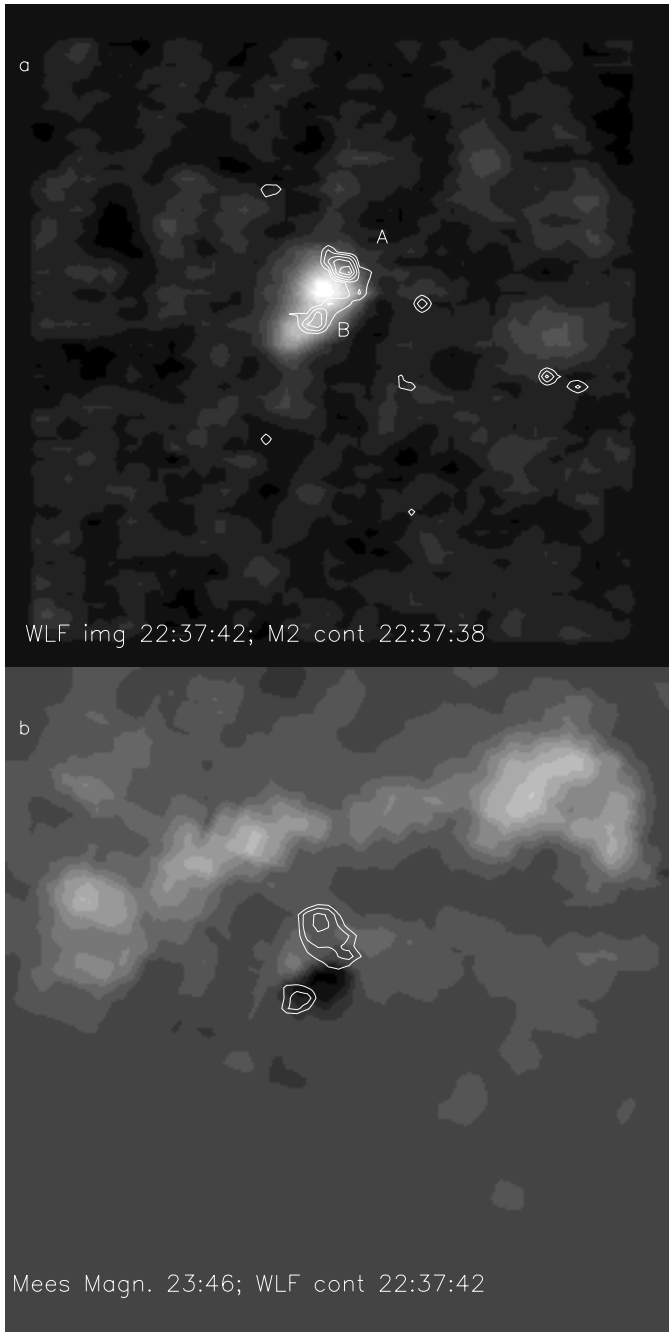

Fig. 5. A mosaic of images showing in a) a grey scale image of the WLF at 22:37:42 UT on 15 Nov. 1991 overlaid with contours of M2 emission at 22:37:38 UT. b) shows the location of the WLF contours in relation to the magnetogram. Each image in the mosaic is $628'' \times 628''$.

4. Results

15 November 91

The hard X-ray flare commenced with a precursor phase at 22:34 UT on November 15 1991 in active region NOAA 6919 (S14W19). *Yohkoh* observed this flare from the start until the end of the HXR emission above 20 keV at 22:44 UT. Flare mode was triggered at 22:34:38 UT. This event has been studied extensively in hard X-rays by Sakao (1994). The white-light flare emission began around 22:36:40 UT as can be seen in Fig. 1. The top of Fig. 5 shows an image of the white-light emission at 22:37:42 UT overlaid with contours of the corresponding hard X-ray sources in the M2 channel at 22:37:38 UT. This event showed double source structure both in hard X-rays and in white-light. The bottom image shows the WLF contours on top of the magnetogram.

We can see from Fig. 5 that there is a close spatial correspondence between the white-light and hard X-ray emission, suggestive of a connection between the origins of the two emissions. Fig. 2 shows the temporal relationship between the two.

Sakao (1994) showed that the footpoints of the double hard X-ray source were located on either side of the magnetic neutral line, and that the brighter of the hard X-ray sources, *A*, is located in a region of positive polarity with longitudinal magnetic field strength, $B \sim +200G$, whilst the dimmer source, *B*, is located in a region of negative polarity with longitudinal field strength $B \sim -400G$ (Sakao 1994).

We now examine the correspondence between the white-light flare and the onset of the ion-acoustic instability, i.e. the point where the drift speed, v_D exceeds the ion-sound speed v_{is}.

In all cases $R = v_D/v_{is}$ has been calculated at the level in active region P model of Basri et al. (1979) in which the return current was shown to be most unstable to the onset of ion-acoustic wave generation. For this level we have $N = 5.0 \times 10^{20}\text{cm}^{-2}$, $n_H = 3.476 \times 10^{13}$ cm^{-3}, $x = 1.784 \times 10^{-3}$ and $T = 5.35 \times 10^3$ K. This level would be appropriate for type I WLFs, formed in the chromosphere.

The white-light emission at the position of the upper hard X-ray footpoint *A* begins at $\sim$ 22:37:00 UT (Fig. 6), as determined by calculating the time at which the fractional signal reaches a level greater than 3σ above a background level. We can see from Fig. 6 that the criterion $R > 1$ is satisfied at around 22:37:00 UT, within the error limits given by the determination of v_D. The white-light emission reaches its peak at $\sim$ 22:37:40 UT, whilst R shows a double peak at approximately this time. By $\sim$22:41:00 UT the HXR emission has returned to background levels in all but the lowest channel of HXT and we see that the white-light emission is also close to pre-flare background levels.

For the lower footpoint, *B*, we see that the white-light emission begins at 22:36:24 UT (see Fig. 6). From the HXR analysis we see that $R > 1$ is satisfied at 23:36:40 UT, some 16s after the start of the white-light flare. The peak value of R is attained at 22:37:30 UT in this case and the maximum of the white-light at 22:37:40 UT.

In both cases we note that there are multiple peaks observed in R, as might be expected from an examination of the hard X-ray light curve. Particularly after the impulsive phase it would appear that small peaks in R are related to the still high level of white-light emission observed until around 22:41 UT. Given the combination of the time resolution of the white-light images and the error bars these timings are probably consistent.

26 January 1992

The flare began at 15:23 UT in NOAA active region 7012 (S16W66). *Yohkoh* observed this flare until 15:43 UT. This event showed five white-light flare patches, *A*, *B*, *C*, *D* and *E* and five hard X-ray sources as can be seen in the upper portion of Fig. 7. The bottom shows the contours of the WLF on top of the magnetogram.

Fig. 8 shows the temporal evolution of $R(= v_D/v_{is})$ and the WLF emission in each of the white-light patches and corresponding hard X-ray sources. For kernels *A*, *B* and *C* $R > 1$ is satisfied between 20-50 seconds before the onset of WLF emission, while for kernels *D* and *E* the threshold is exceeded at a time consistent with the onset of the WLF emission. In these cases the peak of R and the WLF emission can also seen to be to be coincident, within the resolution of the data.

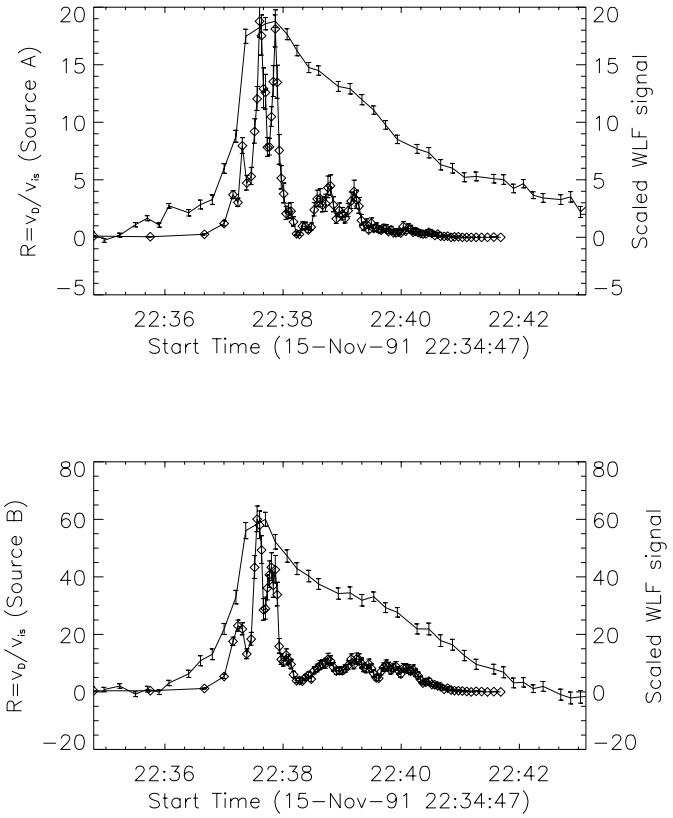

Fig. 6. The variation of $R = v_D/v_{is}$ (diamonds) with time for footpoint A of November 15 1991, calculated at the $N = 5.0 \times 10^{20}$ cm^{-2} level in model atmosphere P of Basri et al. (1979). Overplotted is the light curve from the corresponding white-light kernel. This has been scaled. Below this is a similar plot for source B.

27 October 1991

The flare began at 05:37 UT and flare mode was triggered at 05:37:35 UT. However, the flare began during a data gap and the first hard X-ray data available are from 05:39:25 UT. This flare also ended during a data gap, which makes it impossible to determine a background level by which to estimate the start time of the WL emission. Hence, for this flare, we take the start time to be first frame of the WLF cube.

The hard X-ray emission displayed five sources, *A*, *B*, *C*, *D* and *E*, with 5 coincident sources also visible in the white-light. This coincidence can be seen in Fig. 9, which shows a grey-scale image of the white-light emission at 05:40:35 UT overlaid with HXR contours from the M2 channel at 05:40:01 UT, in the image. Unfortunately, there was no available magnetogram for this region on 27 Oct. 1991. The bottom portion of Fig. 9 shows the HXR contours (white) and WLF contours (black) plotted on a soft X-ray image of the event.

In Fig. 10 the relationship between R and the WLF emission is shown for each of the sources *A*-*E*. The temporal coincidence between the onset of ion-acoustic instability and the start of the

Fig. 7. A mosaic of images showing a) a grey scale image of the WLF at 15:28:41 UT on 26 Jan 1992 overlaid with contours of M2 emission at 15:26:23 UT. b)shows the location of the WLF contours in relation to the magnetogram. Each image in the mosaic is $628'' \times 628''$.

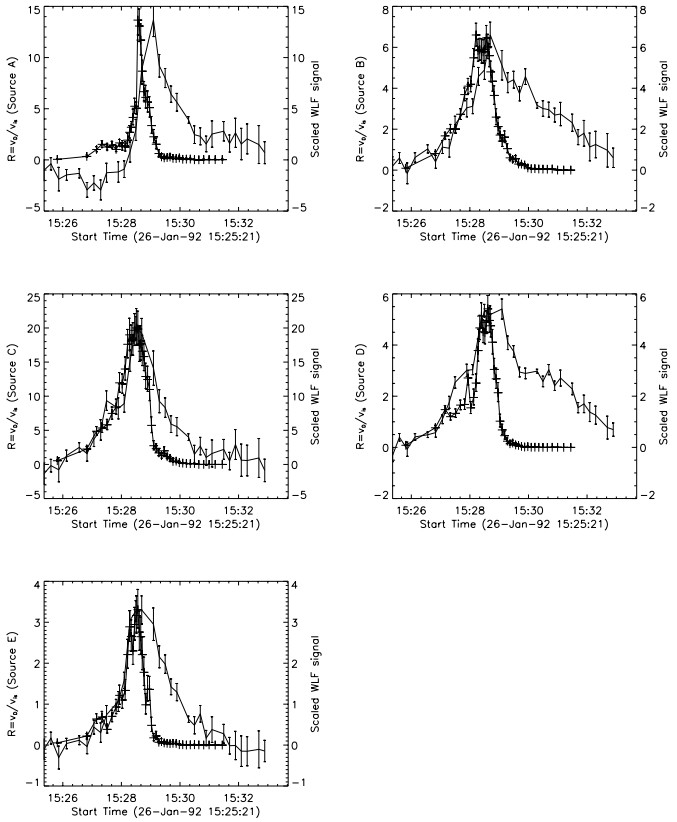

Fig. 8. The variation of $R = v_D/v_{is}$ (+) with time for kernel A of 26 January 1992, calculated at the $N = 5.0 \times 10^{20}$ cm^{-2} level in model atmosphere P of Basri et al. (1979). Overplotted is the light curve from the corresponding white-light kernel. This has been scaled. Similar plots for kernels B, C, D and E are also shown.

WLF emission shows the two to be simultaneous for sources *A*, *B*, *D* and *E*, while R first exceeds unity some 15 seconds before the WLF for source *C*. However, this is still consistent within the time resolution of the WLF data.

14 February 1992

The flare of 14 February 1992 began at 23:04 UT and ended during a data gap after 23:10 UT. This is a particularly interesting white-light event from the point of view that it is an M flare, indicating that white-light emission can appear in flares of size smaller than has been previously thought. Traditionally these events have been associated with very energetic X class flares, but here we see that this is most likely a detection threshold selection effect. This event also showed five distinct sources in both hard X-rays and white-light, as can be seen in Fig. 11. In Fig. 12 we can see that for all five sources the threshold for the onset of ion-acoustic instability is exceeded at a time coincident with the start of the WLF emission.

5. Discussion

It is obvious from the results of this analysis that there are some cases in which the spatial coincidence between the hard X-ray sources and the WLF kernels is not as close as it might be. There are also a number of cases in which the relative timing between the onset of ion-acoustic instability and the start of the white-light emission is subject to a delay on the order of some 10s of seconds. In at least one of these cases, kernel A of 26 January

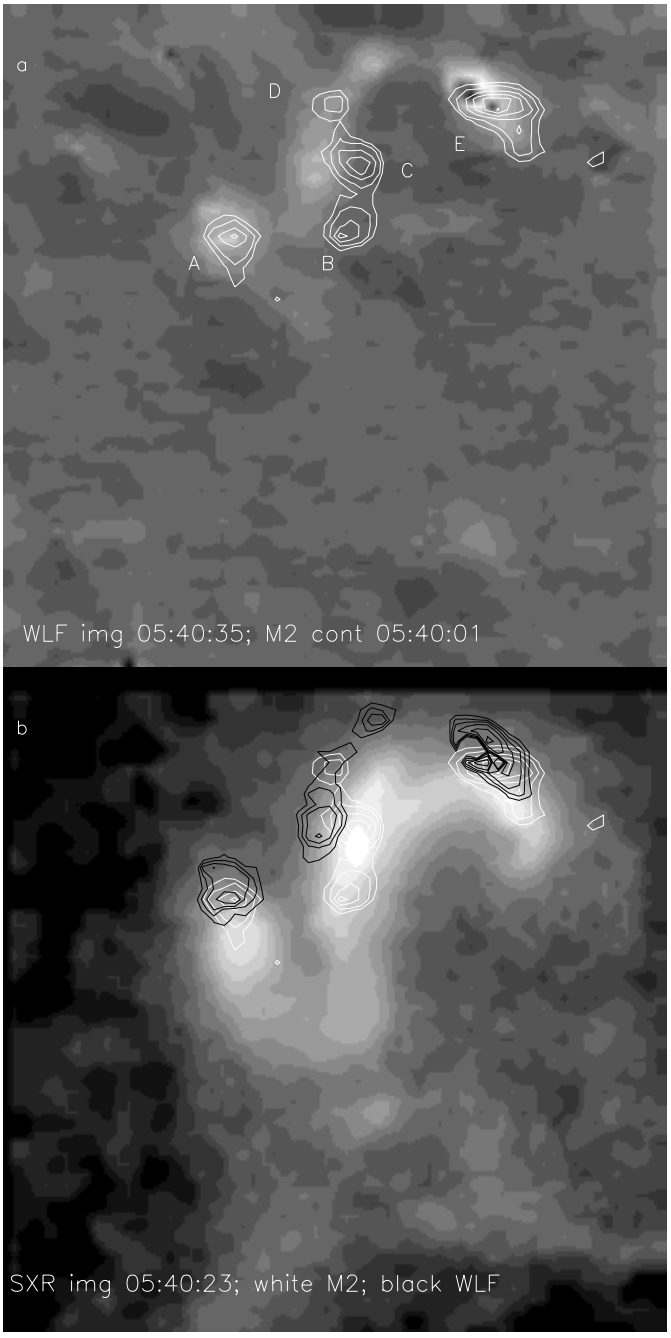

Fig. 9. A mosaic of images showing in a) a grey scale image of the WLF at 05:40:35 UT on 27 Oct. 1991 overlaid with contours of M2 emission at 05:40:01 UT. b) shows the location of the WLF (black) and M2 (white) contours in relation to an SXR image at 05:40:23. Each image in the mosaic is $628'' \times 628''$.

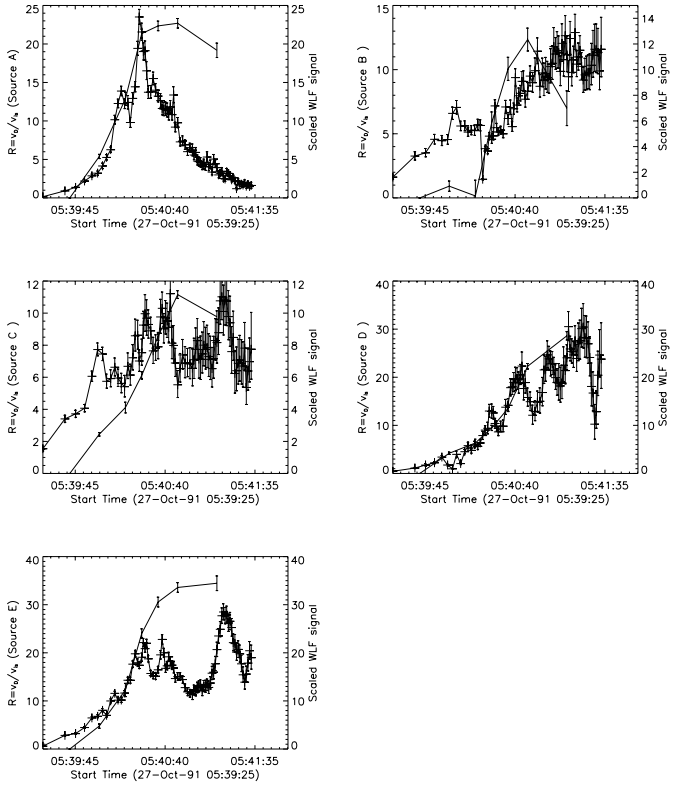

Fig. 10. The variation of $R = v_D/v_{is}$ (+) with time for kernel A of 27 October 1991, calculated at the $N = 5.0 \times 10^{20}$ cm^{-2} level in model atmosphere P of Basri et al. (1979). Overplotted is the light curve from the corresponding white-light kernel. This has been scaled. Similar plots for kernels B, C, D and E are also shown.

1992, the spatial coincidence between the white-light and hard X-ray sources is apparently very good. However, there are certainly a number of cases in each event in which it appears that the observations are consistent with our hypothesis, particularly when we take into account the difference in time resolution between our white-light and hard X-ray observations and the errors associated with data analysis. As discussed in the introduction two types of WLF have been identified from ground-based observations; type I and type II events. The type I events are those which would occur in the deep chromosphere while the type II events suggest that the source of the WLF must be in the upper photosphere. When examining the possibility that the beam return current system might become unstable to the generation of ion-acoustic waves we have considered only one level in a model atmosphere corresponding to the deep chromosphere. Thus, we would expect that we would only find good agreement in those cases where the WLF kernels are of chromospheric origin. If the WLF is actually a combination of both type I and Type II emission we would then expect to find a number of cases which could not be explained by this model.

If we accept that the proposed model passes acceptably the tests of source location and timing, it is then necessary to consider whether it is physically viable. Calculation of the detailed evolution of the wave level in a weakly ionised stratified plasma under the action of the beam return current system and the feedback of the wave level on the beam and return current is beyond the scope of the present paper, which is mainly observational. For example the rising temperature and ionisation due to anomalous dissipation will reduce R and tend toward turning off the instability or moving it to a marginally stable state, reducing the wave level and the anomalous heating rate. Analysis of such evolution should be carried out along similar lines to the work

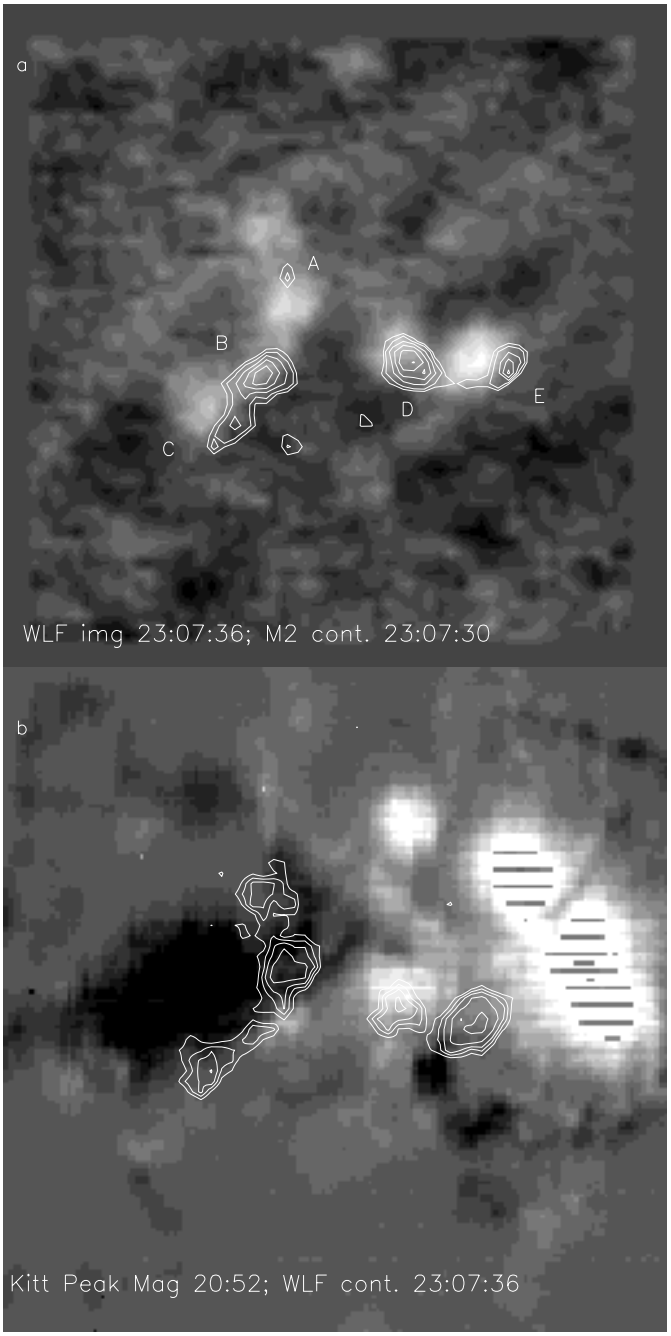

Fig. 11. A mosaic of images showing in a) a grey scale image of the WLF at 23:07:36 UT on 14 Feb. 1992 overlaid with contours of M2 emission at 23:07:30 UT. b) shows the location of the WLF contours in relation to the magnetogram. Each image in the mosaic is $628'' \times 628''$.

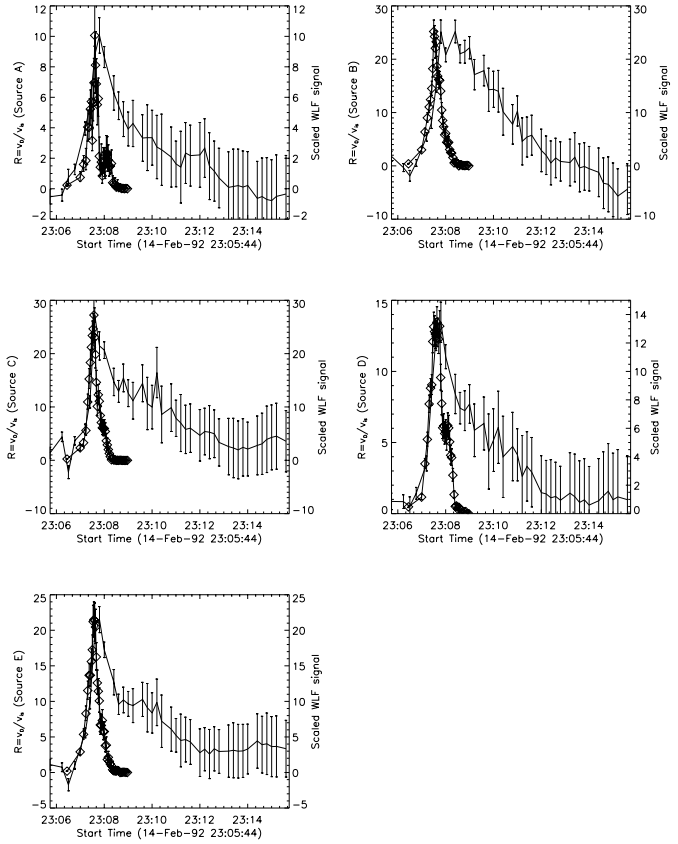

Fig. 12. The variation of $R = v_D/v_{is}$ (diamonds) with time for kernel A of 14 Feb. 1992, calculated at the $N = 5.0 \times 10^{20}$ cm^{-2} level in model atmosphere P of Basri et al. (1979). Overplotted is the light curve from the corresponding white-light kernel. This has been scaled. Similar plots for kernels B, C, D and E are also shown.

of Duijveman et al (1981), Cromwell et al (1988) and van den Oord (1990) extending it to the weakly ionised case. What we will do, however, is to estimate whether the anomalous heating rate would be adequate for WLF production for plausible wave levels and typical observed beam and atmospheric parameters. As before we adopt a beam flux spectrum at acceleration $F_o(E_o) = (\delta - 1)F_1/E_1(E_o/E_1)^{-\delta}$ for $E_o \geq E_1$ where F_1 is the total beam flux at $E_o \geq E_1$. For depths $N \geq N_1 = E_1^2/2K$ we then find for the beam flux F_N and energy flux P_N where it enters the unstable region at depth N

$$F_N(cm^{-2}s^{-1}) = F_1 \left[\frac{N}{N_1}\right]^{-\frac{\delta-1}{2}} \tag{6}$$

$$P_N(ergcm^{-2}s^{-1}) = \frac{\delta-1}{\delta-2} F_1 E_1 \left[\frac{N}{N_1}\right]^{-\frac{\delta-2}{2}} \tag{7}$$

The anomalous ohmic heating rate by the return current is then

$$p_{AN}(ergcm^{-3}s^{-1}) = \frac{w}{(nx)^{1/2}} \eta_{AN} e^2 F_N^2 \tag{8}$$

where the anomalous resistivity is

$$\eta_{AN} = \frac{m_e \nu_{eff}}{2e^2 n_e} = (\frac{\pi m_e}{e^2})^{1/2} \frac{w}{(nx)^{1/2}} \tag{9}$$

where we have taken the effective collision frequency ν_{eff} to be $\nu_{eff} = w\omega_e$ where $w = W/nkT$ is the relative wave energy density and ω_e is the angular plasma frequency for the free electron density nx so that

$$p_{AN} = (\pi m_e e^2)^{1/2} F_1^2 \left[\frac{N}{N_1}\right]^{-\delta+1} \tag{10}$$

From Sect. 4, typical observed values for the HXR emitting beam are $F_1 = 3 \times 10^{18}$ cm^{-2}s^{-1} for $E_1 = 20keV$ and $\delta \approx 4$ while the target atmosphere parameters in the region where $R \geq 1$ are $n \approx 3 \times 10^{13}$cm^{-3}, $x \approx 2 \times 10^{-3}$ with $N \approx 5 \times 10^{20}$ cm^{-2} and $N_1 \approx 10^{20}$ cm^{-2}. For these values the total beam energy flux entering the $R \geq 1$ region is $P_N \approx 2 \times 10^{10}$ erg cm^{-2}s^{-1} which, at 30% of the photospheric flux, is ample for a WLF, and the anomalous heating rate is

$$p_{AN} \approx 10^3 \frac{w}{10^{-3}} ergcm^{-3}s^{-1} \quad (11)$$

so that a relative wave level w exceeding 10^{-3} is sufficient to yield the estimated volumetric heating rate required for a WLF (cf Sect. 2). These values correspond to a characteristic stopping distance $\approx P_N/p_{AN} \approx 10^7$ cm. These estimates support the plausibility of the model and indicate that detailed analysis of the wave generation process will be well worthwhile.

Acknowledgements. SAM would like to thank PPARC for postdoctoral funding. LvDG gratefully acknowledges funding from the Royal Society. SAM and LvDG would also like to acknowledge the support of the Royal Society collaboration program. We would also like to acknowledge the financial support of a UK PPARC Grant (JCB), studentship (SAM) and Visitor Grant (LvDG). We thank the *Yohkoh* Team for the SXT and HXT data and the Mees Observatory staff for the Mees Stokes polarimeter data. Mees Solar Observatory is supported by NASA grant NAGW 1542 to the University of Hawaii. NSO/Kitt Peak magnetograms used in this paper were produced cooperatively by NSF, NOAO, NASA GSFC and NOAA/SEL, courtesy Karen L. Harvey.

References

Basri G.S, Linsky J.L, Bartoe J.-D., Brueckner G.E., Van Hoosier M.E., 1979, ApJ 230, 924
Brown J.C., 1971, Solar Phys. 18, 489
Brown J.C., 1972, Solar Phys. 26, 441
Brown J.C., 1973, Solar Phys. 31, 143
Brown J.C., 1974, Solar Phys. 36, 371
Brown J.C., Melrose D.B., 1977, Solar Phys. 52, 117
Canfield R.C., Bely-Dubau F., Brown J.C., et al., 1986, Energetic Phenomena on the Sun, eds. M. Kundu and B. Woodgate, NASA CP 2439, Chap. 3
Cromwell D., McQuillan P., Brown J.C., 1988, Solar Phys. 115, 289
Culhane J.L., Phillips A.T., Pike C.D., et al., 1993, Adv. Space Res. 13, 303
Duijveman A., Hoyng P., Ionson J.A., 1981, ApJ 245, 721
Emslie A.G., Sturrock P.A., 1982, Solar Phys. 80, 113
Emslie A.G., Brown J.C., MacKinnon A.L., 1997, ApJ 485, 430
Gull S.F., Daniell G.J., 1978, Nature 272, 686
Hénoux J.-C., Chambe G., 1990, Journal of Quantitative Spectroscopy and Radiative Transfer 44, 193
Hoyng P., van Beek H.F., Brown J.C., 1976, Solar Phys. 48, 197
Hudson H.S., van Driel-Gesztelyi L., Kosugi T., 1994, Proc. of Kofu Symposium, NRO Report No. 360, 397
Hurley K., Sommer M., Atteia J.-L., et al., 1992, A&AS 92, 401
Kane S.R., Chupp E.L., Forrest D.J., Share G.H., Rieger E., 1986, ApJ, 300L, 95
Kawabata K., Yoshimori M., Suga K., et al., 1994, ApJS 90, 701
Kosugi T., Makishima K., Murakami T., et al., 1991, Solar Phys. 136, 17
McIntosh P., Donnelly R.F., 1972, Solar Phys. 23, 444
McTiernan J.M., Kane S.R., Loran J.M., et al., 1994, X-Ray Solar Physics from Yohkoh, eds. Y. Uchida et al., 255
Machado M.E., Emslie A.G., Brown J.C., 1978, Solar Phys. 58, 363
Machado M.E., Emslie A.G., Mauas P.J., 1986, A&A 159, 33
Machado M.E., Emslie A.G., Avrett E.A., 1989, Solar Phys. 124, 303
Matthews S.A., Brown J.C., Melrose D.B., 1996, A&A L305, 49
Mauas P.J.D., Machado M.E., Avrett, E.H., 1990, ApJ 360, 715
Morrison M., 1994, The Yohkoh Analysis Guide
Neidig D.F., 1986, The Lower Atmosphere of Solar Flares, ed. D.F. Neidig
Neidig D.F., 1989, Solar Phys. 121, 361
Neidig D.F., Cliver E.W., 1983, Air Force Geophysics Lab. Technical Report AFGL-TR-83-0257
Neidig D.F., Wiborg D.H., 1984, Solar Phys. 94, 217
Neidig D.F., Kane S.R., 1993, Solar Phys. 143, 201
Poland A.I., Milkey R.W., Thompson W.I., 1988, Solar Phys. 115, 277
Ramaty R., Mandzhavidze N., Kozlovsky B., Murphy R., 1995, ApJ L455, 193
Rieger E., Neidig D.F, Engfer D.W., Strelow D., 1996, Solar Phys. 167, 307
Ryan J.M., Chupp E.L., Forrest D.J., et al., 1983, ApJ 227L, 61
Sakao T., 1994, PhD. Thesis, University of Tokyo
Schmeleva O.P., Syrovatskii S.I., 1973, Solar Phys. 33, 341
Simnett G.M., 1986, Solar Phys. 106, 165
Spitzer L., 1962, Physics of Fully Ionized Gases, Interscience
Švestka Z., 1986, The Lower Atmosphere of Solar Flares: Proceedings of the Solar Maximum Symposium, 332
Uchida Y., Hudson H.S., 1972, Solar Phys. 26, 414
van den Oord G.H.J., 1990, A&A 234, 496
van Driel-Gesztelyi L., Hudson H.S., Anwar B., Hiei E., 1994, Solar Phys. 152, 145
Vogt E., Sahal-Brechot S., Hénoux J.C., 1997, A&A 324, 1211
Willingdale R., 1981, MNRAS 194, 359
Yoshimori M., Suga K., Morimoto K., et al., 1994, ApJS 90, 639
Zhao X., Fang C., Hénoux J.C., 1998, A&A 330, 351